Cirera, B., Sánchez-Grande, A., de la Torre, B. et al. Tailoring topological order and π-conjugation to engineer quasi-metallic polymers. Nat. Nanotechnol. 15, 437–443 (2020). https://doi.org/10.1038/s41565-020-0668-7

https://www.nature.com/articles/s41565-020-0668-7

Tailoring topological order and π-conjugation to engineer quasi-metallic polymers

Borja Cirera,[1,†] Ana Sánchez-Grande,[1,†] Bruno de la Torre,[2,3,†] José Santos,[1,6] Shayan Edalatmanesh,[3] Eider Rodríguez-Sánchez,[1,6] Koen Lauwaet,[1] Benjamin Mallada-Faes,[3] Radek Zbořil[3], Rodolfo Miranda,[1,5] Oliver Gröning,[4,*] Pavel Jelínek,[2,3*] Nazario Martín,[1,6*] and David Ecija[1,*]

Affiliations:

[1]IMDEA Nanociencia. 28049 Madrid, Spain.

[2]Institute of Physics. The Czech Academy of Sciences, 162 00 Prague, Czech Republic.

[3]Regional Centre of Advanced Technologies and Materials. Palacký University, 78371 Olomouc, Czech Republic.

[4]nanotech@surfaces laboratory. EMPA - Swiss Federal Laboratories for Materials Science and Technology, 8600 Dübendorf, Switzerland

[5]Departamento de Física de la Materia Condensada. Facultad de Ciencias. Universidad Autónoma de Madrid, 28049 Madrid, Spain.

[6]Departamento de Química Orgánica. Facultad de Ciencias Químicas. Universidad Complutense de Madrid, 28040 Madrid, Spain.

*Correspondence to: oliver.groening@empa.ch (O.G), jelinekp@fzu.cz (P.J.), nazmar@quim.ucm.es (N.M.), david.ecija@imdea.org (D.E.)

† Equally contributing authors.

Abstract:

Topological band theory predicts that a topological electronic phase transition between two insulators must proceed via closure of the electronic gap. Here, we use this transition to circumvent the instability of metallic phases in π-conjugated 1D polymers. By means of density functional theory, tight binding and GW calculations, we predict polymers near the topological transition from a trivial to a non-trivial quantum phase. We then use on-surface synthesis with custom-designed precursors to make polymers consisting of 1D linearly bridged acene moieties, which feature narrow bandgaps and in-gap zero-energy edge-states when in the topologically non-trivial phase close to the topological transition point. We also reveal the fundamental connection between topological classes and resonant forms of 1D π-conjugated polymers.

π-conjugated polymers have received particular interest from scientists and industry alike, since the discovery of high conductivity in doped polyacetylene showed that it was possible to create organic synthetic metals[1]. Such finding opened the new field of what is known today as organic electronics[2]. At the same time, intense research at the boundary between chemistry and condensed-matter physics was triggered, which contributed to progress in understanding the fundamental chemistry and physics of π-conjugated macromolecules[3]. Notably, the relation between topological band theory and conduction in doped polyacetylene (PA) was soon introduced by the Su-Shrieffer-Heeger (SSH) model[4]. Steered by this discovery, great efforts have been devoted during last decades to rationally relate chemical structure and electronic properties in these materials[5]. In this regard, gaining control over the bandgap of π-conjugated polymers has been a target of particular interest[6,7]. Such bandgap depends mainly upon the molecular structure of the repeating unit. Accordingly, synthetic chemists have been provided with the opportunity and the challenge of tuning the bandgap by design at the molecular level, only precluded by synthetic limitations, such as solubility[8]. Hereby, a great attention is devoted to reduce or even quench the bandgap. Narrow bandgap π-conjugated polymers are of utmost interest because of their potential for near-infrared applications, high conductivity, and ambipolar charge transport character[9,10,11]. Furthermore, the synthesis of intrinsic conductive π-conjugated polymers has remained elusive. One strategy towards this challenge is to design π-conjugated polymers with a small energy difference between the aromatic and quinoidal resonant structures simultaneously reducing the band gap[12,13,14,15]. However, despite the efforts devoted, nowadays the only feasible way to enhance the conductivity of polymers (as for PA) is via doping (either chemically or electrochemically), although the process is known to be detrimental to their stability[3].

The rapid development of on-surface synthesis has emerged as a new paradigm for engineering nanomaterials[16,17,18], while it also circumvents the solubility limitations associated to synthetic wet-chemistry. The might of this novel approach was recently exemplified by graphene nanoribbons[19], whereby robust topological SSH quantum phases were rationally engineered[20,21]. Although on-surface synthesis was up to now primarily concerned with graphene derived nanostructures, for future applications it will be also desirable to design long, defect-free and transferable[22,23,24,25] 1D π-conjugated polymers.

Following this on-surface synthetic paradigm, we have just reported the pathway to engineer surface-confined ethynylene-bridged anthracene polymers featuring high π-conjugation[26]. Inspired by this recent discovery and based on the roots of topological band theory, we introduce here the theoretical basis and the experimental demonstration of the rational engineering of one-dimensional polymers that are located near the quantum phase transition from topological trivial to non-trivial class, thus featuring a narrow bandgap. Such polymers are topologically non-trivial and consequently exhibit in-gap zero-energy edge-states.

Prediction of a topological phase transition in acene polymers

The concept of a structure related topological phase transition and the corresponding bandgap closure is exemplified in Fig. 1a for the structure family of linearly-bridged acene polymers. Tight-binding (Fig. 1b), density functional theory (DFT) and GW calculations (Supplementary Fig. 1) show a monotonic decrease of the HOMO (highest occupied molecular orbital) - LUMO (lowest unoccupied molecular orbital) gap of the acene monomer as a function of the acene size (where *n* denotes the number of benzene rings of the acene species)[27], as expected from the

increasing delocalization of the frontier orbitals. However, the band gap of the ethynylene-bridged polymers shows a distinctly non-monotonic behaviour, which is characterized by the closure of the bandgap for the pentacene polymer (n=5) and its reopening for larger acenes (n>5). The topological analysis of the polymers, by determination of the Zak phase, reveals that the closure of the bandgap is associated with a transition of the topological class of the polymers from trivial Z_2=0 to non-trivial Z_2=1 (see Supplementary Notes 1-3 and Supplementary Figs. 3-5 for details of the topological analysis and definition of the topological invariant Z_2 in this case). The sequence of the linearly-bridged acene polymers can therefore be understood as representing a topological phase transition in the discrete variable n denoting the acene size. According to topological band theory such a phase transition must come along with a metallic, i.e. zero bandgap interface. Figure 1 shows that this transition happens near a specific structure ('near', because n cannot vary continuously), which is the ethynylene-bridged pentacene polymer (n = 5). As discussed in the following, experiments indeed show that the pentacene polymer has a narrow bandgap. Furthermore, it also features characteristic in-gap zero-energy edge-states, evidencing that it is located just at the onset of the non-trivial topological phase region (Fig. 1a).

This topological transition in the polymer can be tentatively understood in terms of the dimerized atomic chain described by the SSH model[28] (see Supplementary Note 4 and Supplementary Figs. 6-9). Here, the gap between valence band $E_-(k)$ and conduction band $E_+(k)$, with $E_\pm(k) = \pm\sqrt{t_1^2 + t_2^2 + 2t_1t_2\cos(k)}$, vanishes when $|t_1| = |t_2|$, i.e. when the intra-cell coupling strength within the dimers t_1 matches the inter-cell coupling strength t_2 between the dimers. The situation $|t_1| > |t_2|$ yields a topological trivial and $|t_1| < |t_2|$ a topological non-trivial insulator respectively.

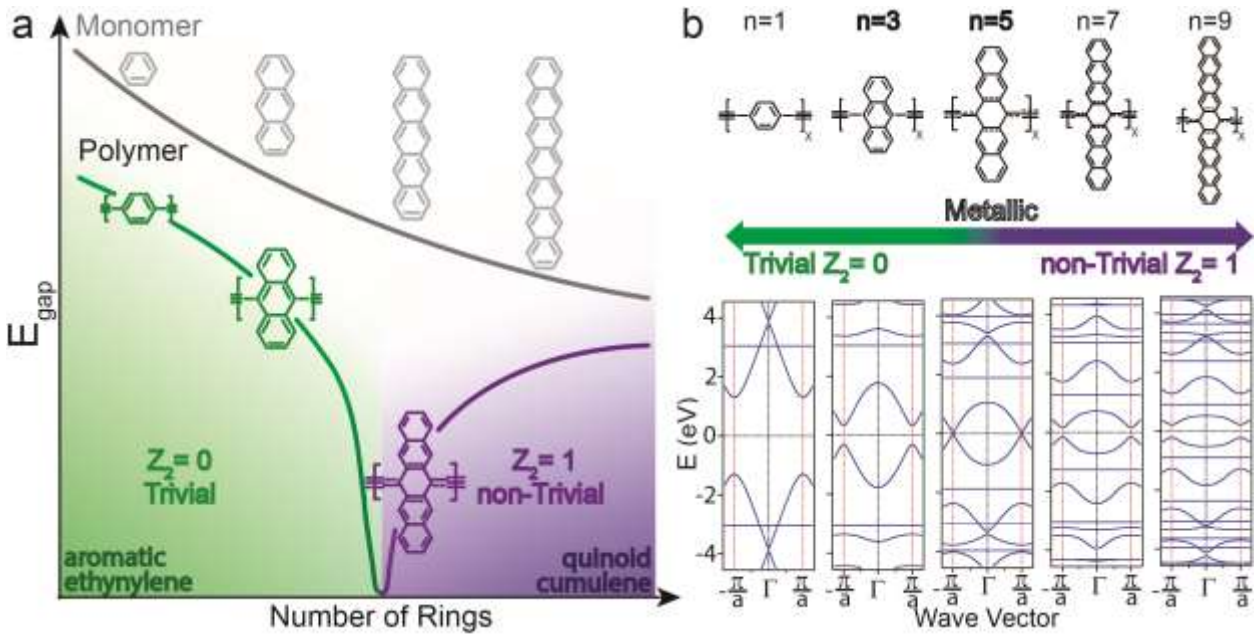

Fig. 1. **Topological quantum phase transition in the acene polymer family. a,** Schematic evolution of the bandgap of acene monomers and polymers with increasing size of acene monomer. The latter case shows a phase transition between trivial and non-trivial topological classes accompanied by transformation of the π-conjugation of the polymer. The band gap evolution with size of acenes for both monomers and polymers obtained from DFT calculations is shown in Figure S1. **b,** Band diagram (E vs. wave vector) for the ethynylene linked acene polymers obtained from tight binding calculations revealing strong renormalization of the band gap near the topological phase transition.

Translating this situation to the acene polymer case means to associate the HOMO and LUMO orbital of an isolated acene unit to the bonding and antibonding SSH dimer states respectively. The HOMO-LUMO gap is then directly related to the intra-cell coupling strength. The inter-cell coupling, provided by a single atomic bond in the SSH model, is provided by the ethynylene-bridge in our polymers (see Supplementary Note 4 and Supplementary Figs. 6-9 for details of this concept). For small acenes, the HOMO-LUMO gap is large and the intra-cell coupling (t_1) exceeds the inter-cell coupling (t_2), which results is a topologically trivial insulating phase (n = 1 and n = 3 in Fig. 1). As the size of the acene unit increases, the HOMO-LUMO gap decreases, and the intra-cell coupling starts matching the inter-cell coupling, which results in the closure of

the bandgap (n=5). Further increase of the acene size makes the inter-cell coupling (t_2) overcome the intra-cell one (t_1), resulting in a change of the topological class and a reopening of the bandgap.

Remarkably, as we will justify later, the polymers described here may adopt two distinct arrangements of the π-conjugated structure (resonant forms), either the acene monomers being fully aromatic and linked through ethynylene bridges or the acene blocks adopting a quinoid structure connected by cumulene linkers (see Fig. 1a). Our results reveal that the ground state of the polymers is composed by a distinct mixture of the two distinct resonant forms. For small acenes ($n < 5$) the dominant form is the aromatic-ethynylene structure, whereas for higher acenes ($n \geq 5$) the dominant structure is the quinoid-cumulene form. Along this manuscript, we will demonstrate that the topological phase transition of the acene polymers is related to a change in the dominant resonant form, as illustrated in Figure 1a.

On-surface synthesis of topologically non-trivial one-dimensional polymers.

In order to experimentally implement the outlined strategy, we have used on-surface synthesis to produce two different polymers of the acene structural family. We synthesized the required molecular precursors **4BrAn** (9,10-bis(dibromomethylene)-9,10-dihydroanthracene) and **4BrPn** (6,13-bis(dibromomethylene)-6,13-dihydropentacene) (see Methods section for synthetic details). These precursors bear the $=CBr_2$ functionality. Such terminal group has been recently used to steer skeletal rearrangements on NaCl by voltage pulses[29] or to induce homocoupling through a set of chemical reactions on Au(111)[30], as recently exemplified by us for **4BrAn**[26]. The periodic homocoupling of the precursors gives rise to the formation of anthracene (n = 3) and pentacene (n = 5) polymers, whose structural and electronic characterization is summarized in Figs. 2 and 3.

The deposition of a submonolayer coverage of **4BrAn** or **4BrPn** on Au(111) and subsequent annealing at 500 K results in the emergence of long polymeric wires (see Supplementary Fig. 10). Residual bromine atoms detached from the precursors are fully removed from the substrate at this temperature. High resolution nc-AFM imaging with CO-functionalized tip[31] reveals that polymers are planar and formed by intact anthracene (Fig. 2a,b) and pentacene (Fig. 3a,b) moieties, and linked by linear bridges (Figs. 2b and 3b). Defects within the polymer chains are scarce (see Supplementary Fig. 10 for long range images of the different polymers). The polymerization eventually terminates once the entire $=CBr_2$ group is lost and the acene backbone passivated by residual atomic hydrogen.

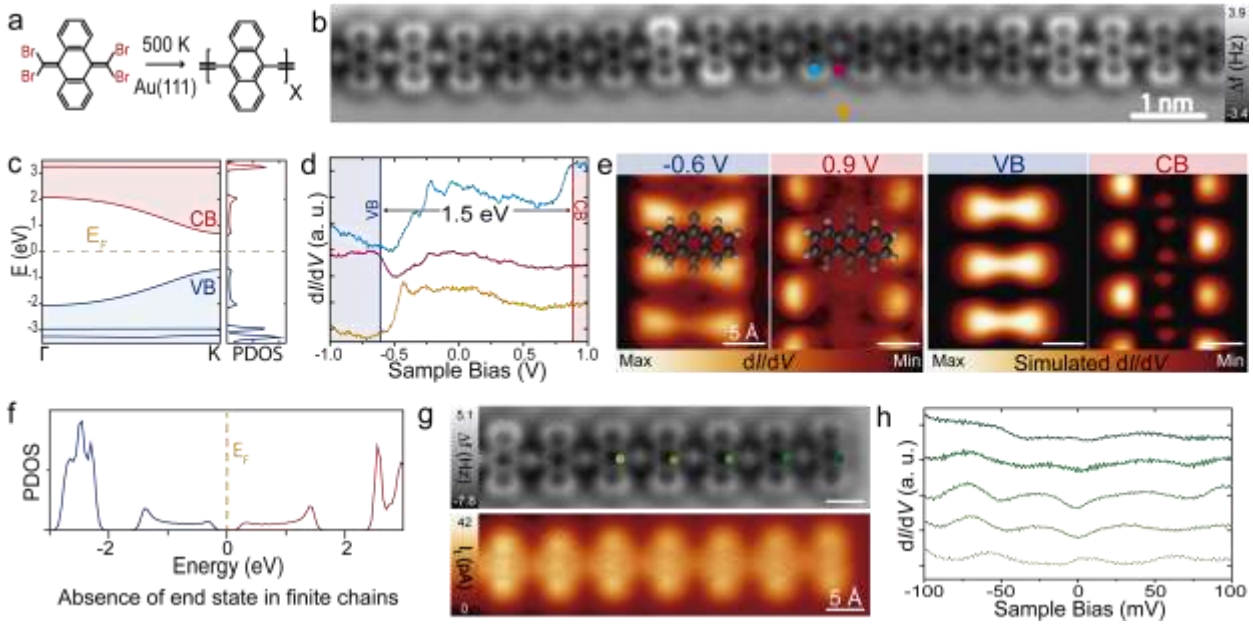

Fig. 2. Experimental and theoretical results for anthracene (*n* = 3) polymer[26]. **a**, Chemical sketch of the resulting polymer for *n* = 3. **b,** nc-AFM image of the *n* = 3 polymer. **c**, Bulk calculated band structure and PDOS. **d**, Experimental determination of E_{gap} with STS acquired at the positions depicted in **b**. **e,** Constant current dI/dV maps acquired at the approximate energies of the VB and CB (left) with the corresponding simulated maps (right). Notice that the valence band (VB) and conduction band (CB) edges are not located in the same position in space, the VB edge appearing in between anthracene moieties, and the CB edge on top of them. The VB edge does not show maxima over the anthracene moieties, but it has states over the bridges and, remarkably, also on the voids adjacent to the links. The CB edge, on the contrary, exhibits states located over the edges of the anthracene moieties[26]. **f**,

Calculated projected density of states for a finite chain of 15 units, where zero-energy edge-state is not developed. **g,** nc-AFM (top) and constant-height STM (bottom) images of a -H terminated anthracene polymer. **h**, STS point spectra (position depicted in **g**) along the termination, highlighting the absence of edge-state. All imaging and spectroscopy parameters are provided in Supplementary Table 1.

In the case of the anthracene polymer, as recently reported by us[26], the calculated electronic structure using density functional theory (DFT) reveals the presence of dispersive valence (VB) and conduction (CB) bands (Fig. 2c), whereby scanning tunnelling spectroscopy (STS) shows a sizable band gap of ~1.5 eV (Fig. 2d). Calculated band structure and dI/dV maps (Fig. 2e) match very well with the experimental evidence. In addition, the DFT electronic structure of a finite anthracene chain shows the absence of end-states (Fig. 2f and Supplementary Fig. 11) and inspection of the hydrogen terminated ends of the polymer show no signatures of an in-gap topological edge-state (Fig. 2g-h). These findings demonstrate that the anthracene polymer is in a topologically trivial electronic phase, as predicted in Fig. 1a.

In the case of pentacene precursor (n=5), the reaction (Fig. 3a) proceeds as previously described, achieving planar polymers with linearly linked pentacene moieties (Fig. 3b). DFT calculations display the presence of dispersive valence and conduction bands (Fig. 3c). STS shows two resonances at -150 meV and 200 meV (Fig. 3d), which we assign to the edge of the valence (VB) and conduction bands (CB), respectively (Fig. 3e). This results in the narrow bandgap of ~0.35 eV. We should note that the band gap value obtained from STS measurements is typically reduced by additional electron screening imposed by the presence of an underlying metallic surface with respect to the intrinsic band gap of polymer in gas phase[32,33]. The proximity to the topological transition within the structure family (Fig. 1) makes it highly susceptible to strong relative band gap renormalization. This can be induced e.g. by structural relaxations (by influencing the bond length) or by the environment independently of screening effects (see details in Supplementary Note 5 and Supplementary Fig. 12). Consequently, the band gap of the

polymer in gas phase with respect to the one placed on a metallic surface can be further reduced if it is found closer to the topological phase transition. This scenario is supported by quasiparticle GW calculations of the free-standing pentacene polymer, which predict nearly metallic band gap $E_g \sim 0.05\ eV$ and opening again of the band gap for polymers with larger acene units (see Supplementary Note 5).

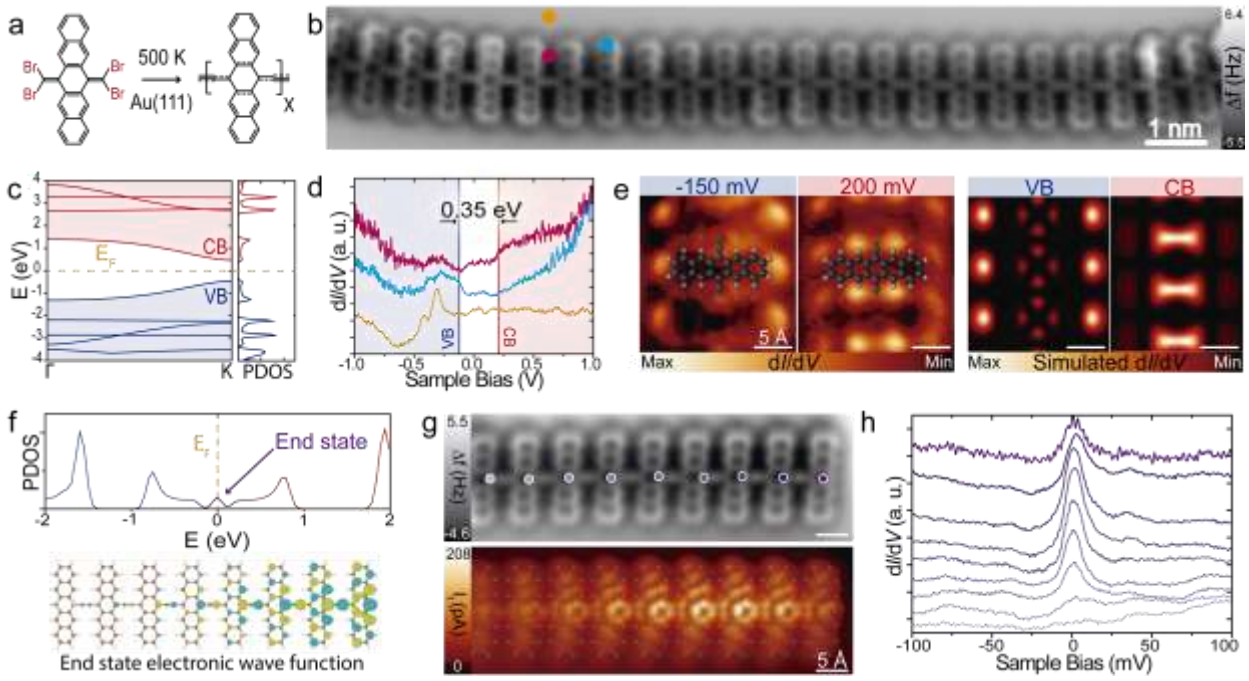

Fig. 3. Experimental and theoretical results for pentacene (*n* = 5) polymer. **a**, Chemical sketch of the resulting polymer for *n* = 5. **b,** nc-AFM image of the *n* = 5 polymer. **c**, Bulk calculated band structure and PDOS. **d**, Experimental determination of E_{gap} with STS acquired at the positions depicted in **b**. **e,** Constant current dI/dV maps acquired at the approximate energies of the VB and CB (left) with the corresponding simulated maps (right). The VB edge shows states located over the edges of the pentacene moieties, while CB edge has intensity maxima over the coupling bridges and on the voids adjacent to them. **f,** Calculated projected density of states for a finite chain of 15 units, where a close to zero-energy edge-state emerges as a consequence of the non-trivial topology. **g**, Constant height nc-AFM (top) and STM (bottom) images of a -H terminated pentacene polymer, highlighting the fading away of the edge-state. **h**, STS spectra along the termination (position depicted in **g**) showing the vanishing of the edge-state. All imaging and spectroscopy parameters are provided in Supplementary Table 1.

Despite the fact that DFT simulations cannot predict correctly the magnitude of the intrinsic band gap of the polymer[34], they well describe the character of frontiers orbitals of the VB and CB edges of both polymers. Indeed, the agreement between experimental and simulated dI/dV maps is excellent, validating the character of the frontiers orbitals predicted by DFT calculations (see Figures 2e and 3e). Interestingly, the character of the CB dI/dV maps of the pentacene polymer is similar to VB dI/dV maps of anthracene polymer and vice versa. This electronic swap plays a critical role in the understanding of the topological phase and the electronic transformation of the π-conjugated polymers, as we will show in the next section.

Regarding the topological class of the pentacene polymer, the DFT calculation predicts the presence of in-gap zero-energy edge-states at the hydrogen terminated end of finite polymer chains (Fig. 3f and Supplementary Fig. 11), thus positioning it in the non-trivial region of the structural phase diagram. Experimentally, this end-state is indeed readily observed as a strong resonance by STS at the Fermi level as shown in Fig. 3g-3h, corroborating its non-trivial topological nature. The small experimental bandgap is further supported by the large extent of the edge-state wave function, which is inversely related to the size of the bandgap (see discussion in Supplementary Information). It should be noted that the weight distribution of the edge-states does not follow the expected exponential decay at the first few segments. This effect is tentatively assigned to variations of the bond strengths due to relaxations at the polymer ends, a view supported by tight binding simulations (see details in Supplementary Note 6 and Supplementary Figs. 13-15).

In the case of the pentacene polymer, both GW and DFT calculations (Supplementary Fig. 1) and experiment show a finite size bandgap, whereas TB suggests a basically vanishing gap, see Fig. 1b. In the simplistic TB model, totally rigid bonds that do not depend on the specific electronic

structure of the polymer and that do not consider structure relaxation are assumed. Therefore, we cannot expect the TB model to represent the true ground state of the system, particularly in polymeric structures which can adopt different π-conjugated forms, as discussed below.

Next, we show that our concept of achieving narrow bandgap polymers by tuning their structure to the topological phase boundary can be extended to other structure families. To this end, we adopted the same on-surface synthesis strategy as before to form bisanthene polymers on Au(111) surface, this time using the **4BrBiA** (10,10'-bis(dibromomethylene)-10*H*,10'*H*-9,9'-bianthracenylidene) precursor (Fig. 4a), which belongs to the fused acenes family.

The deposition of a submonolayer coverage of **4BrBiA** on Au(111) and subsequent annealing at 500 K gives rise to the emergence of long polymeric wires (Fig. 4a,b and Supplementary Fig. 10). As illustrated by high resolution AFM imaging with CO-tip the polymers are planar and formed by bisanthene moieties linked by linear bridges, i.e. we keep the same bridge structure, but change to a larger repeating unit.

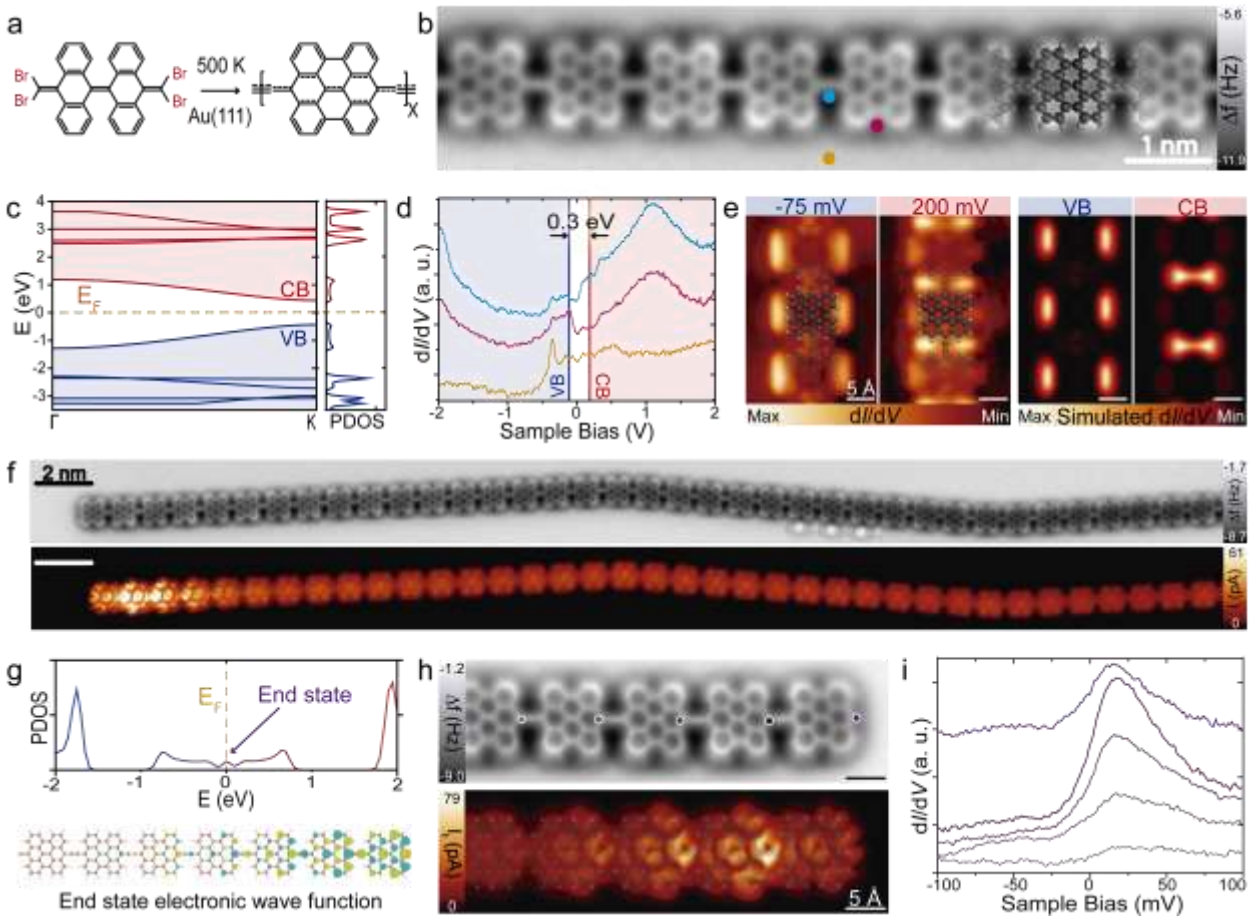

Fig. 4. **Experimental and theoretical results for topologically non-trivial bisanthene polymers**. **a,** Reaction pathway on Au(111). **b,** nc-AFM image of the resulting polymer with the superimposed model. **c,** Bulk calculated band structure and PDOS. **d,** Experimental determination of E_{gap} with STS with the position highlighted in **b**. **e,** Constant current dI/dV maps acquired at the approximate energies of the VB and CB (left) with the corresponding simulated maps (right). The dI/dV map at the VB edge shows maxima over the borders of the bisanthene units, whereas the CB edge displays a bowtie shape over the linear linkers and adjacent voids, and some states over the bisanthene lateral borders. **f,** Large-scale constant height nc-AFM and STM images showing the edge-state resulting from the non-trivial topological character of the polymer. **g,** Calculated projected density of states for a finite chain of 15 units, where a close to zero-energy edge-state emerges as a consequence of the non-trivial topology. **h,** Constant height nc-AFM (top) and STM (bottom) images of a -H terminated polymer, highlighting the fading away of the edge-state. **i,** STS spectra along the termination showing the existence and distribution of the edge-state. All imaging and spectroscopy parameters are provided in Supplementary Table 1.

Again, the excellent agreement between experimental STS measurements and DFT calculations allows the unambiguous determination of the bulk electronic structure of the polymer (Fig. 4c). Experimental STS spectra recorded over the polymers on the Au(111) surface show two frontier resonances close to the Fermi level, at - 75meV (edge of VB) and 200 meV (edge of CB) (Fig. 4d) giving a narrow bandgap of ~0.3 eV. Interestingly, the dI/dV maps of the VB and CB edges have similar symmetry as the pentacene polymer.

Both TB and GW calculations of the fused acenes polymer family reveal that the topological phase transition, with a nearly vanishing gap (smaller 0.05 eV), is expected at n = 3, i.e. the bisanthene polymer (Supplementary Figs. 1, 16 and 17). DFT calculations predict a larger band gap (Supplementary Fig. 1) and the presence of edge-states for the finite structures (Fig. 4g and Supplementary Fig. 11). The latter is in full correspondence with the observation the zero-energy edge-states in the experiment (Figs. 4h, i). In analogy to the pentacene case, the bisanthene polymer is located close to the topological transition in the non-trivial region.

Relation between resonant form and topological quantum phase of π-conjugated polymers

At this stage, it is important to realize that polymers described here may adopt two extreme resonant forms, either the bridge being an alkyne (ethynylene) and the acene fully aromatic or the bridge being a cumulene and the acene adopting a quinoid structure (see Fig. 1a and Supplementary Fig. 18). In combination with the small gap this raises the question of a Jahn-Teller or Peierls type structural instability forcing an opening of the band gap. Herein, it is important to highlight that the ground state of these polymers is composed by different mixture of the two π-conjugated forms instead of their pure states[35] depending on the acene moiety size, with only one global minimum along the variation of the resonant form from aromatic-

ethynylene towards quinoid-cumulene according to the DFT simulations (see Supplementary Note 7 and Supplementary Fig. 19). As a result, the existence of the single global minimum opens up a possibility to tune the system to achieve the metallic state.

The symmetry of the frontier orbitals seen in the dI/dV maps is not the only similarity shared by the topologically non-trivial bisanthene and pentacene polymers. High-resolution AFM images acquired with CO-tip[31,36] also show several similarities, which are not present in the case of the anthracene polymers. Namely, the nc-AFM images of the anthracene polymer display the triple bond as a faint protrusion (see Fig. 2 and Supplementary Fig. 20), revealing the presence of the ethynylene $-C \equiv C-$ arrangement of the linear bridge, as recently illustrated for one-dimensional molecular wires[26,37]. However, in the case of the pentacene and bisanthene polymers, the triple bond signature in the bridges is absent as shown on Figs. 3, 4 and Supplementary Fig. 20, indicating increasing cumulene $(= C = C =)$ character of the bridge.

These findings highlight that the anthracene polymer adopts the ethynylene-aromatic structure of the π-conjugation, while the two topologically non-trivial polymers prefer the cumulene/quinoid-like form. Such results are also supported by a thorough analysis of the DFT simulations of the bond length variations (see explanation in Supplementary Note 8 and Supplementary Fig. 21) and of the charge density isocontour plots compared with the high resolution nc-AFM images (see details in Supplementary Note 9 and Supplementary Fig. 22).

The transition between aromatic/quinoid and ethynylene/cumulene character in π-conjugated polymers was rationalized by the level crossing, where HOMO/LUMO frontier orbitals of distinct symmetry swap[35,38]. A detailed analysis of the frontier orbitals character of all three polymers confirms this scenario (see Supplementary Fig. 23). Namely, in the case of the anthracene polymer, the highest occupied wave function at K-edge of the Brillouin zone shows

π-bonding character between the two C atoms forming the triple bond, reinforcing the ethynylene $-C \equiv C -$ character. However, in the case of the pentacene and bisanthene polymer, the wave function with this symmetry is found as the lowest unoccupied orbital. This rationalizes the weakening of the triple bond. This effect, together with a relatively small energy difference between the two π-conjugated forms facilitates the promotion of the cumulene-quinoid over ethynylene-aromatic form. Importantly, the level crossing of the frontier orbitals accompanying the electronic π-conjugated transition changes the nodal character of the frontier wave functions forming the conduction band. Consequently, this gives rise to a change of the Zak phase identifying the transition of the topological phase (see underlying discussion in Supplementary Notes 2-4). Thus, we conclude that there is a direct relation between the topological and the π-conjugated transition.

It has been demonstrated that the aromatic character of acene monomers tends to π-electron confinement within the rings while the quinoid character promotes delocalization of π-electrons along the polymer. Therefore, polymers consisting of acene monomers linked by ethynylene/cumulene bridges open playground for the competition between π-electron localization within acene rings and delocalization along the bridges[39]. For small acene monomers with large band gap, the ground state aromatic form has much lower energy than the quinoid form. Under such circumstances, the polymers prefer to adopt the ethynylene-aromatic π-conjugation form as the ground state. However, with increasing size of the acene monomers, the energy difference between the aromatic and quinoid structure becomes small, lowering the energy penalty for promoting the cumulene/quinoid π-conjugation form along the polymer. At a certain size of the acene monomer, the enhanced contribution of the cumulene/quinoid π-conjugation in the ground state structure of the polymer causes the level crossing and the

polymers transform into the topologically non-trivial phase. The situation when two frontier orbitals involved in the crossing level mechanism become degenerated corresponds exactly to the topological phase transition featuring the metallic character. In the topologically trivial phase, the enhancement of the cumulene/quinoid π-conjugation leads to decrease of the band gap value, whereas in the topologically non-trivial phase this causes its increase and the appearance of the zero-energy edge-states within the gap. Thus, it is evident that the size of the bandgap is determined by the proximity to the topological phase transition, i.e. the variation of the crossing level with degenerated frontier orbitals.

Conclusions

We establish the fundamental relation between topological quantum phases and change of resonant forms in π-conjugated polymers. We predict a topological phase transition in the families of linearly bridged acene and fused acenes polymers while increasing the size of the monomer. By exploiting on-surface chemical protocols we engineer π-conjugated polymers exhibiting unique electronic properties featuring narrow bandgaps and in-gap zero-energy edge-states when in the topological non-trivial quantum phase close to the topological transition point. We envision that these polymers could find applications in a wide variety of areas including molecular electronics, optoelectronics, organic solar cells and quantum information technology[40].

Furthermore, we anticipate that from the conceptual framework described here the band gap could be tuned by a clever chemical design, targeting to position the polymer the closest as possible to the topological transition point, with the final goal of synthesizing intrinsic metallic polymers, i.e. achieving metallic character without chemical or electrochemical doping[41]. In

addition, intrinsic conducting polymers could revive efforts in condensed matter physics such as the quest for high Tc organic superconductors[42], the expression of Tomonaga-Luttinger liquid behaviour in polymers, or the deeper understanding of the metal-to-insulator Mott transition in organic nanomaterials[41].

Methods

Synthesis of molecular precursors

The molecular precursors were synthesized following minor modifications of the general Ramirez-Corey-Fuchs protocol for synthesizing alkynes from carbonyls. General procedure: a solution of carbon tetrabromide (4 equiv.) and triphenylphosphine (8 equiv.) in dry toluene was stirred at room temperature for 30 min. Thereafter, corresponding quinone (1 equiv.) was added in one portion and the resulting mixture refluxed for 24/48 h upon completion (monitoring by TLC). Reaction products were purified by column chromatography (silica gel as stationary phase and hexane as eluent). The characterization of all **4BrAn**, **4BrPn**[43] and **4BrBiA**[44] products is in agreement with their reported spectroscopic features.

Sample preparation and STM/STS/nc-AFM measurements

Experiments were performed in two independent custom designed ultra-high vacuum systems that host a low-temperature Omicron and a Createc scanning tunnelling microscope, respectively, where the base pressure was below 5×10^{-10} mbar. STM images were acquired with electrochemically etched tungsten tips, or cut and sharpened by focus ion beam (FIB) Pt/Ir tips, applying a bias (V_b) to the sample at a temperature of ~4 K. The Au(111) substrate was prepared by standard cycles of Ar^+ sputtering (800 eV) and subsequent annealing at 723 K for 10 minutes.

Molecular precursors were deposited by organic molecular-beam epitaxy (OMBE) from a quartz crucible maintained at 373 K (**4BrAn**), 423 K (**4BrPn**) or 443 K (**4BrBiAn**) onto a clean Au(111) held at room temperature. Whenever necessary samples were annealed to the desired temperature and subsequently transferred to the STM stage, which was maintained at 4 K. In nc-AFM imaging, a Pt/Ir tip mounted on a qPlus sensor (resonant frequency ≈ 30 kHz; stiffness ≈ 1800 N/m) was oscillated with a constant amplitude of 50 pm. The tip apex was functionalized with a CO-molecule, and all images were captured in constant height mode.

DFT and GW calculations of electronic structure

Density Functional Theory calculations for all freestanding finite and infinite systems (anthracene, pentacene and bisanthene) are done using FHI-AIMS, Fireball packages[45]. All geometry optimizations and electronic structure analyses have been performed twice, using two different exchange-correlation functionals: PBE[46] and B3LYP[47]. Systems were allowed to relax until the remaining atomic forces reached below 10^{-2} eV/Å. We also performed many-body non self-consistent G_oW_o calculations to obtain quasiparticle spectra of infinite polymers implemented within the FHI-AIMS package with default values. In these G_oW_o calculations, the initial single particle wave functions and the optimized geometries were obtained using the GGA-PBE exchange-correlation functional. For all infinite systems with periodic boundary condition (PBC), a Monkhorst-Pack grid of 18x1x1 was used to sample the Brillouin zone. Theoretical dI/dV maps were calculated by DFT Fireball[48] program package and PPSTM code with Probe Particle SPM code[49] a s-like orbital tip[50].

Data availability

The data that support the plots within this paper and other findings of this study are available from the corresponding author upon reasonable request.

Code availability

The Tight Binding calculations have been performed using a custom made code on the Wave Metrics IGOR Pro platform. Details of this TB code can be obtained from the corresponding author upon reasonable request

References and Notes

1 Chiang, C. K. *et al.* Electrical conductivity in doped polyacetylene. *Phys. Rev. Lett.* **39**, 1098-1101 (1977).

2 Farchioni, R. & Grosso, G. *Organic electronic materials: conjugated polymers and low molecular weight organic solids*. (Springer, 2001).

3 Heeger, A. J. Semiconducting and metallic polymers: The fourth generation of polymeric materials (Nobel Lecture). *Angew. Chem. Int. Ed.* **40**, 2591-2611 (2001).

4 Heeger, A. J., Kivelson, S., Schrieffer, J. R. & Su, W. P. Solitons in conducting polymers. *Rev. Mod. Phys.* **60**, 781-850 (1988).

5 Facchetti, A. π-Conjugated polymers for organic electronics and photovoltaic cell applications. *Chem. Mater.* **23**, 733-758 (2011).

6 Roncali, J. Synthetic Principles for Bandgap Control in Linear π-Conjugated Systems. *Chem. Rev.* **97**, 173-206 (1997).

7 Roncali, J. Molecular Engineering of the Band Gap of π-Conjugated Systems: Facing Technological Applications. *Macromol. Rapid Commun.* **28**, 1761-1775 (2007).

8 Chujo, Y. *Conjugated polymer synthesis: Methods and reactions*. (WILEY-VCH, 2010).

9 Steckler, T. T. *et al.* Very low band gap thiadiazoloquinoxaline donor–acceptor polymers as multi-tool conjugated polymers. *J. Am. Chem. Soc.* **136**, 1190-1193 (2014).

10 Dou, L., Liu, Y., Hong, Z., Li, G. & Yang, Y. Low-bandgap near-IR conjugated polymers/molecules for organic electronics. *Chem. Rev.* **115**, 12633-12665 (2015).

11 Kawabata, K., Saito, M., Osaka, I. & Takimiya, K. Very small bandgap π-conjugated polymers with extended thienoquinoids. *J. Am. Chem. Soc.* **138**, 7725-7732 (2016).

12 Scherf, U. & Müllen, K. Design and synthesis of extended pi-systems: Monomers, oligomers, polymers. *Synthesis* **1-2**, 23-38 (1992).

13 Garay, R. O., Naarmann, H. & Muellen, K. Synthesis and characterization of poly(1,4-anthrylenevinylene). *Macromolecules* **27**, 1922-1927 (1994).

14 Taylor, P. N., Wylie, A. P., Huuskonen, J. & Anderson, H. L. Enhanced electronic conjugation in anthracene-linked porphyrins. *Angew. Chem. Int. Ed.* **37**, 986-989 (1998).

15 Susumu, K., Duncan, T. V. & Therien, M. J. Potentiometric, electronic structural, and ground- and excited-state optical properties of conjugated bis[(porphinato)zinc(II)] compounds featuring proquinoidal spacer units. *J. Am. Chem. Soc.* **127**, 5186-5195 (2005).

16 Talirz, L., Ruffieux, P. & Fasel, R. On-surface synthesis of atomically precise graphene nanoribbons. *Adv. Mater.* **28**, 6222-6231 (2016).

17 Shen, Q., Gao, H.-Y. & Fuchs, H. Frontiers of on-surface synthesis: From principles to applications. *Nano Today* **13**, 77-96 (2017).

18 Gross, L. *et al.* Atomic force microscopy for molecular structure elucidation. *Angew. Chem. Int. Ed.* **57**, 3888-3908 (2018).

19 Cai, J. *et al.* Atomically precise bottom-up fabrication of graphene nanoribbons. *Nature* **466**, 470-473 (2010).
20 Rizzo, D. J. *et al.* Topological band engineering of graphene nanoribbons. *Nature* **560**, 204-208 (2018).
21 Gröning, O. *et al.* Engineering of robust topological quantum phases in graphene nanoribbons. *Nature* **560**, 209-213 (2018).
22 Bennett, P. B. *et al.* Bottom-up graphene nanoribbon field-effect transistors. *Appl. Phys. Lett.* **103**, 253114 (2013).
23 Llinas, J. P. *et al.* Short-channel field-effect transistors with 9-atom and 13-atom wide graphene nanoribbons. *Nat. Commun.* **8**, 633 (2017).
24 Moreno, C. *et al.* Bottom-up synthesis of multifunctional nanoporous graphene. *Science* **360**, 199 (2018).
25 Borin Barin, G. *et al.* Surface-synthesized graphene nanoribbons for room temperature switching devices: substrate transfer and ex situ characterization. *ACS Appl. Nano Mater.* **2**, 2184-2192 (2019).
26 Sánchez-Grande, A. *et al.* On-surface synthesis of ethynylene bridged anthracene polymers. *Angew. Chem. Int. Ed.* **58**, 6559-6563 (2019).
27 Bettanin, F. *et al.* Singlet La and Lb bands for N-acenes (N = 2–7): A CASSCF/CASPT2 Study. *J. Chem. Theory Comput.* **13**, 4297-4306 (2017).
28 Asbóth, J. K., Oroszlány, L. & Pályi, A. in *A Short course on topological insulators: band structure and edge states in one and two dimensions*, 1-22 (Springer International Publishing, 2016).
29 Pavliček, N. *et al.* Polyyne formation via skeletal rearrangement induced by atomic manipulation. *Nat. Chem.* **10**, 853-858 (2018).
30 Sun, Q. *et al.* On-surface formation of cumulene by dehalogenative homocoupling of alkenyl gem-dibromides. *Angew. Chem. Int. Ed.* **56**, 12165-12169 (2017).
31 Gross, L., Mohn, F., Moll, N., Liljeroth, P. & Meyer, G. The chemical structure of a molecule resolved by atomic force microscopy. *Science* **325**, 1110 (2009).
32 Neaton, J. B., Hybertsen, M. S. & Louie, S. G. Renormalization of molecular electronic levels at metal-molecule interfaces. *Phys. Rev. Lett.* **97**, 216405 (2006).
33 Amy, F., Chan, C. & Kahn, A. Polarization at the gold/pentacene interface. *Org. Electron.* **6**, 85-91 (2005).
34 Cohen, A. J., Mori-Sánchez, P. & Yang, W. Insights into current limitations of density functional theory. *Science* **321**, 792 (2008).
35 Kertesz, M., Choi, C. H. & Yang, S. Conjugated polymers and aromaticity. *Chem. Rev.* **105**, 3448-3481 (2005).
36 Jelínek, P. High resolution SPM imaging of organic molecules with functionalized tips. *J. Phys: Condens. Matter* **29**, 343002 (2017).
37 Kawai, S. *et al.* Diacetylene linked anthracene oligomers synthesized by one-shot homocoupling of trimethylsilyl on Cu(111). *ACS Nano* **12**, 8791-8797 (2018).
38 Karpfen, A. Ab initio studies on polymers. IV. Polydiacetylenes. *J. Phys. C* **12**, 5673 (1980).
39 Hernandez, V., Castiglioni, C., Del Zoppo, M. & Zerbi, G. Confinement potential and pi-electron delocalization in polyconjugated organic materials. *Phys. Rev. B* **50**, 9815-9823 (1994).

40 Estarellas, M. P., D'Amico, I. & Spiller, T. P. Topologically protected localised states in spin chains. *Sci. Rep.* **7**, 42904 (2017).
41 Heeger, A. J. Semiconducting and metallic polymers: The fourth generation of polymeric materials. *J. Phys. Chem. B.* **105**, 8475-8491 (2001).
42 Little, W. A. Possibility of synthesizing an organic superconductor. *Phys. Rev.* **134**, A1416-A1424 (1964).
43 Gorodetsky, A. A. *et al.* Reticulated heterojunctions for photovoltaic devices. *Angew. Chem. Int. Ed.* **49**, 7909-7912 (2010).
44 Zeng, Z. *et al.* Stable tetrabenzo-Chichibabin's hydrocarbons: Tunable ground state and unusual transition between their closed-shell and open-shell resonance forms. *J. Am. Chem. Soc.* **134**, 14513-14525 (2012).
45 Blum, V. *et al.* Ab initio molecular simulations with numeric atom-centered orbitals. *Comput. Phys. Commun.* **180**, 2175-2196 (2009).
46 Perdew, J. P., Burke, W. & Ernzerhof, M. Generalized gradient approximation made simple. *Phys. Rev. Lett.* **77**, 3965 (1996).
47 Becke, A. D. Density-functional thermochemistry. III. The role of exact exchange. *J. Chem. Phys.* **98**, 5648 (1998).
48 Lewis, J. P. *et al.* Advances and applications in the FIREBALL ab initio tight-binding molecular-dynamics formalism. *Phys. Status Solidi B* **248**, 1989-2007 (2011).
49 Hapala, P. *et al.* Mechanism of high-resolution STM/AFM imaging with functionalized tips. *Phys. Rev. B* **90**, 085421 (2014).
50 Krejčí, O., Hapala, P., Ondráček, M. & Jelínek, P. Principles and simulations of high-resolution STM imaging with a flexible tip apex. *Phys. Rev. B* **95**, 045407 (2017).

Acknowledgments

Work supported by the ERC Consolidator Grant ELECNANO (nº 766555), the EC FP7-PEOPLE-2011-COFUND AMAROUT II, the Spanish Ramón y Cajal programme (nº RYC-2012-11133), the Spanish Ministerio de Economía y Competitividad (projects FIS 2013-40667-P, FIS 2015-67287-P), and the Comunidad de Madrid (projects QUIMTRONIC-CM (Y2018/NMT-4783), MAD2D (S2013/MIT-3007), NANOFRONTMAG (S2013/MT-2850), and PHOTOCARBON (S2013/MIT-2841)). Support from the European Research Council (ERC-320441-Chirallcarbon) and the MINECO of Spain (projects CTQ2017-83531-R and CTQ2016-81911-REDT) is also acknowledged. IMDEA Nanociencia thanks support from the "Severo Ochoa" Programme for Centers of Excellence in R&D (MINECO, Grant SEV-2016-0686). P.J. acknowledges support from Praemium Academie of the Academy of Science of the Czech Republic, MEYS LM2015087 and GACR 18-09914S and Operational Programme Research, Development and Education financed by European Structural and Investment Funds and the Czech Ministry of Education, Youth and Sports (Project No. CZ.02.1.01/0.0/0.0/16_019/0000754). P.J. and S. E. acknowledge access to computing and storage facilities owned by parties and projects contributing to the Czech National Grid Infrastructure MetaCentrum provided under the programme "Projects of Large Research, Development, and Innovations Infrastructures" (CESNET LM2015042).

Author Contribution

P.J., N.M., and D.E. conceived and designed the experiments. O.G., P.J., N.M, and D.E. supervised the project and led the collaboration efforts. B.C., A.S-G., B.T., and D.E. carried out the experiments and obtained the data. J.S., E.R.-S. and N. M. synthesized the precursors. The experimental data were analyzed by B.C., A.S.-G., B.T., B.M-F., R.Z., R.M., O.G., P. J. and D.E., and discussed by all the authors. S. E. and P.J. performed the DFT and GW calculations. O.G. carried out the tight binding calculations. The manuscript was written by B. C., O. G., P. J., N.M. and D. E., with contribution from all the authors.

Competing Interests

The authors declare no competing interests.

Additional Information

Supplementary information is available in the online version of the paper.

Reprints and permissions information is available online at www.nature.com/reprints.

Correspondence and request for materials should be addressed to O.G., P.J., N.M, and D.E.